ELSEVIER

Physica D 108 (1997) 92–112

PHYSICA D

Classification of the solitary waves in coupled nonlinear Schrödinger equations

Jianke Yang [1]

Department of Mathematics and Statistics, The University of Vermont, 16 Colchester Avenue, Burlington, VT 05401, USA

Received 16 September 1996; revised 12 December 1996; accepted 3 February 1997
Communicated by A.C. Newell

Abstract

In this paper, the solitary waves in coupled nonlinear Schrödinger equations are classified into infinite families. For each of the first three families, the parameter region is specified and the parameter dependence of its solitary waves described and explained. We found that the parameter regions of these solution families are novel and irregular, and the parameter dependence of the solitary waves is sensitive. The stability of these families of solitary waves is also determined. We showed that only the family of symmetric and single-humped solitary waves is stable.

Keywords: The coupled nonlinear Schrödinger equations; Solitary waves

1. Introduction

In recent years the system of two coupled nonlinear Schrödinger equations has attracted a great deal of attention. These equations were first derived 30 years ago by Benney and Newell [1] for two interacting nonlinear wave packets in a dispersive and conservative system. Under some simplifications and variable rescaling, these equations can be written as

$$iA_t + A_{xx} + (|A|^2 + \beta|B|^2)A = 0, \tag{1.1a}$$

$$iB_t + B_{xx} + (|B|^2 + \beta|A|^2)B = 0, \tag{1.1b}$$

where A and B represent the complex amplitudes of two wave packets, and β is a real-valued cross-phase modulation coefficient [2]. In the late 1980s, it was realized that Eqs. (1.1) also govern the interaction between waves of different frequencies and between orthogonally polarized components in nonlinear optical fibers [3,4]. The experimental and theoretical investigations on the optical-soliton based telecommunication systems called for a thorough study of

[1] Tel.: 802-656-4314; fax: 802-656-2552; e-mail: jyang@emba.uvm.edu.

PII S0167-2789(97)00035-3

the solution behaviors in these equations. Numerous analytical and numerical work has been done on this problem since then (see [4] and the references therein).

Solitary waves play a special role in the coupled nonlinear Schrödinger equations (1.1). These waves are localized pulses that propagate without change of shape. We have found that they often dominate the long time solution evolution [5,6]. These waves and their stability have been investigated by Mesentsev and Turitsyn [8], Kaup et al. [9], Haelterman and Sheppard [10,11], Haelterman et al. [12], Silberberg and Barad [13], Yang and Benney [5] and Yang [7] among others. The work in [8–10] showed that there exists a family of symmetric, single-humped and stable solitary waves with an arbitrary polarization. The work in [11,12] revealed two more solution families, one of which was numerically shown to be unstable in [13]. In joint work with D. Benney, we found infinite families of solitary waves, three of which are those just mentioned above. Based on some analytical results and numerical evidence, we conjectured that only the family of symmetric single-humped solitary waves is stable. In [7], we studied multi-hump permanent waves in general nonlinear systems. Under some assumptions, we developed simple criteria for constructing such permanent waves. We then applied these results to Eqs. (1.1) and established the existence of countably infinite multi-hump solitary waves in certain parts of the parameter region.

The findings of infinite families of solitary waves in Eqs. (1.1) necessitate a classification of these families in the parameter space. This work will systematically summarize the types of solitary waves that exist and how they depend on the parameters. More importantly, this classification can be used to conclusively determine the stability of the solitary waves. Two solitary waves belong to one family if they can continuously change from one to the other when the parameters vary. Due to continuity, the solitary waves in the same family generally have the same stability behaviors. This enables us to determine the stability of a whole family of solitary waves if the stability of one wave is known. Lastly from the dynamical systems point of view, a solitary wave is a homoclinic orbit connecting the origin to itself in the phase space. The information we obtain from this classification can be used as the basis to further study the homoclinic chaos and spatial complexity of solutions in Eqs. (1.1).

In the remainder of this paper, we will classify the solitary waves in Eqs. (1.1) into various families. As we will see later in the paper, there are infinite families of solitary waves. We will focus on the first three of them. For each family, we will determine its parameter region, which is often highly irregular, and describe the parameter dependence of its solitary waves, which is often very sensitive. We will use a combination of numerical, perturbation and variational principle methods in our investigation. These three methods will reinforce each other and offer information as well as insight into the problem at hand. In the end of this paper, we will discuss the stability of these families of solitary waves.

It should be mentioned that the solitary waves in a nonlinear wave system can also be studied by dynamical systems methods. This has been done for Benney's equation [14]. Such methods have also been used to find the homoclinic and heteroclinic orbits of some Hamiltonian systems [16–18]. It will be interesting to see how the results in this paper can be reproduced by such methods. But those methods are largely qualitative. They may be unable to provide the quantitative information on the parameter region and the parameter dependence of the solitary waves, which can be supplied by the methods used in this paper.

2. Solitary waves

The solitary waves in Eqs. (1.1) have the following general form:

$$A = e^{iUx/2+i(\omega_1^2-U^2/4)t}\, r_1(x-Ut), \tag{2.1a}$$

$$B = e^{iUx/2+i(\omega_2^2-U^2/4)t}\, r_2(x-Ut), \tag{2.1b}$$

where U is the velocity of the wave. Let us denote $\bar{x} = x - Ut$ and $\omega^2 = \omega_2^2/\omega_1^2$. Then after a rescaling of variables

$$\bar{t} = \omega_1^2 t, \quad \bar{r}_1 = r_1/\omega_1, \quad \bar{r}_2 = r_2/\omega_1, \tag{2.2}$$

and the bars dropped, we obtain the following ordinary differential equations for $r_1(x)$ and $r_2(x)$:

$$r_{1xx} - r_1 + (r_1^2 + \beta r_2^2) r_1 = 0, \tag{2.3a}$$

$$r_{2xx} - \omega^2 r_2 + (r_2^2 + \beta r_1^2) r_2 = 0, \tag{2.3b}$$

where $r_1(x) \to 0$ and $r_2(x) \to 0$ as $|x| \to \infty$. This is a nonlinear eigenvalue problem. In this paper we will treat the two parameters β and ω in Eqs. (2.3) as arbitrary positive numbers and call the (β, ω) plane the parameter plane. If one of $r_1(x)$ and $r_2(x)$ is zero, then Eqs. (2.3) can be easily solved. The solutions are

$$r_1 = \sqrt{2}\,\operatorname{sech} x, \quad r_2 = 0 \tag{2.4}$$

and

$$r_1 = 0, \quad r_2 = \sqrt{2}\,\omega \operatorname{sech} \omega x. \tag{2.5}$$

In the remainder of this paper, we will only consider solutions in which both r_1 and r_2 are non-zero. These solutions have the following general properties:

(1) *Symmetry*: If $r_i(x)$ $(i = 1 \text{ or } 2)$ is a solution, so is $-r_i(x)$.

(2) *Translational invariance*: If $[r_1(x), r_2(x)]$ is a solution, so is $[r_1(x - x_0), r_2(x - x_0)]$, where x_0 is an arbitrary constant.

(3) *Reciprocal relation*: If $[r_1(x; \omega), r_2(x; \omega)]$ is a solution, so is

$$\left[\hat{r}_1\left(x; \frac{1}{\omega}\right), \hat{r}_2\left(x; \frac{1}{\omega}\right)\right] = \left[\frac{1}{\omega} r_2\left(\frac{x}{\omega}; \omega\right), \frac{1}{\omega} r_1\left(\frac{x}{\omega}; \omega\right)\right]. \tag{2.6}$$

We call two solitary waves $(r_1^{(a)}, r_2^{(a)})$ and $(r_1^{(b)}, r_2^{(b)})$ equivalent if one of them can be deduced from the other by Property (1) or (2). All equivalent solitary waves will be treated as one. In the following we will classify the solitary waves in Eqs. (2.3) into various families in the parameter plane. A solitary wave is controlled by the parameter values of β and ω. We say that two solitary waves belong to one family if they can continuously change from one to the other when β and ω vary. Property (3) indicates that for each family of solitary waves there is another family related to it. We call one the associated family to the other. Once the information on one family is available, that on its associated family will be automatically obtained. For instance, the parameter region of the associated family consists of points (β, ω) where $(\beta, 1/\omega)$ lies in the parameter region of the original family.

Before we classify the solitary waves for arbitrary values of β and ω, we can first get some important information from special values of β or ω. When $\omega = 1$, Eqs. (2.3) allow the following solitary waves of equal amplitudes

$$r_1 = r_2 = \sqrt{2/(1+\beta)}\,\operatorname{sech} x. \tag{2.7}$$

When $\beta = 1$ and $\omega = 1$, the solutions are

$$r_1 = \sqrt{2}\cos\theta \operatorname{sech} x, \quad r_2 = \sqrt{2}\sin\theta \operatorname{sech} x, \tag{2.8}$$

where θ is an arbitrary parameter. The solutions (2.8) are symmetric, single-humped and have arbitrary polarizations. They form an one-parameter family of solutions. When $\beta = 1$ and $0 < \omega < 1$, the solutions are

$$r_1 = \frac{\sqrt{2(1-\omega^2)}\cosh\omega x}{\cosh(x-\Delta x)\cosh\omega x - \omega\sinh(x-\Delta x)\sinh\omega x}, \tag{2.9a}$$

$$r_2 = \frac{-\omega\sqrt{2(1-\omega^2)}\sinh(x-\Delta x)}{\cosh(x-\Delta x)\cosh\omega x - \omega\sinh(x-\Delta x)\sinh\omega x}, \tag{2.9b}$$

where Δx is an arbitrary parameter [15]. These solutions also form an one-parameter family of solutions for each fixed ω. They are asymmetric in general. However, when $\Delta x = 0$, r_1 becomes symmetric and r_2, anti-symmetric. If $\beta = 1$ and $\omega > 1$, the solutions can be deduced from (2.9) by the reciprocal relation (2.6). When $\beta = 3$ and $\omega = 1$, the solutions are

$$r_1 = \tfrac{1}{2}\sqrt{2}[\operatorname{sech}(x-\Delta x) + \lambda\operatorname{sech}(x+\Delta x)], \tag{2.10a}$$

$$r_2 = \tfrac{1}{2}\sqrt{2}[\operatorname{sech}(x-\Delta x) - \lambda\operatorname{sech}(x+\Delta x)], \tag{2.10b}$$

where $\lambda = 1$ or -1, and Δx is an arbitrary parameter [5]. In these solutions, one of r_1 and r_2 is symmetric and the other anti-symmetric.

Another important category of solitary waves in Eqs. (2.3) is the so-called wave and daughter wave solutions in which either $r_2 \ll r_1$ or $r_1 \ll r_2$. In these solutions, the smaller of r_1 and r_2 is called the daughter wave. The functional forms of such solutions can be approximately obtained as follows [5]. Let us first assume that $r_2 \ll r_1$. Then to the leading order approximation,

$$r_{1xx} - r_1 + r_1^3 = 0, \tag{2.11}$$

and

$$r_{2xx} - \omega^2 r_2 + \beta r_1^2 r_2 = 0. \tag{2.12}$$

Under the condition that $r_1 \to 0$ as $|x| \to \infty$, the solution of Eq. (2.11) is

$$r_1 = \sqrt{2}\operatorname{sech} x, \tag{2.13}$$

which then reduces Eq. (2.12) to

$$r_{2xx} - \omega^2 r_2 + 2\beta\operatorname{sech}^2 x\, r_2 = 0. \tag{2.14}$$

This equation can be transformed into a hypergeometric equation [19]. In order for $r_2 \to 0$ as $|x| \to \infty$, we need to require that

$$\omega = s - n, \tag{2.15}$$

where

$$s = \tfrac{1}{2}(\sqrt{1+8\beta} - 1), \tag{2.16}$$

n is a non-negative integer and $n < s$. For each fixed value of β, there is a finite number of daughter wave solutions for r_2, all of which are either symmetric or anti-symmetric in x. The first solution, which exists for any $\beta > 0$, is

$$r_2 \propto \operatorname{sech}^s x, \qquad \omega = s, \tag{2.17}$$

which is an even function in x. The second solution, which exists when $\beta > 1$, is

$$r_2 \propto \operatorname{sech}^s x \sinh x, \qquad \omega = s - 1, \tag{2.18}$$

which is an odd function in x. The third solution, which exists when $\beta > 3$, is

$$r_2 \propto \operatorname{sech}^s x[1 + 2(1 - s)\sinh^2 x], \qquad \omega = s - 2, \tag{2.19}$$

which is even in x. As $\beta \to \infty$ we will find an infinite number of such solutions. In the parameter plane, the curves given by (2.15) represent the boundaries of wave and daughter wave solutions. If $r_1 \ll r_2$ in the solitary waves, the solutions can be deduced from those described above by the reciprocal relation (2.6). In particular, the wave and daughter wave boundaries now become

$$\omega = 1/(s - n) \tag{2.20}$$

in the parameter plane.

The above exact and approximate solitary wave solutions for special values of β or ω are very helpful in classifying the solitary waves in Eqs. (2.3). First, they suggest that there are infinite families of solitary waves. The evidence is that there is an infinite number of branches of wave and daughter wave solutions as mentioned above, and different branches belong to different families. Second, all the solitary waves at $\beta = 1$ are given by (2.8), (2.9) and the relation (2.6). As we will see later, the line $\beta = 1$ in the parameter plane plays a special role in our classification. Lastly, there are both symmetric, anti-symmetric and asymmetric solitary waves exemplified by (2.8) and (2.9). In the remainder of this paper, we will only examine the symmetric and anti-symmetric solitary waves and carry out their classifications. Asymmetric solitary waves will be considered elsewhere.

3. Families of solitary waves generated by the wave and daughter wave solutions

In this section we classify the families of solitary waves which are generated by the wave and daughter wave solutions. In the parameter plane the parameter regions of these families spread out from the wave and daughter wave boundaries (2.15) or (2.20). Given the infinite families of these solutions, we will focus on the first three of them.

3.1. Family D_1

We call family D_1 as the family of solitary waves which is generated by the first wave and daughter wave solution of the approximate form (2.13) and (2.17). In this family, both r_1 and r_2 of the solutions are symmetric and single-humped. We have determined these solutions numerically by the shooting method. One example is plotted in Fig. 1. In the parameter plane, the two curves

$$\omega = s = \tfrac{1}{2}(\sqrt{1 + 8\beta} - 1) \tag{3.1}$$

and

$$\omega = 1/s = 2/(\sqrt{1 + 8\beta} - 1), \tag{3.2}$$

together with the ω-axis, furnish the boundaries of family D_1's parameter region. This region is shown in Fig. 2. Near the boundaries $\omega = s$ and $\omega = 1/s$, the solitary waves are wave and daughter wave solutions with $r_2 \ll r_1$ and $r_1 \ll r_2$, respectively. For any fixed $\beta > 0$, as ω changes from s to $1/s$, the polarization of the solitary wave

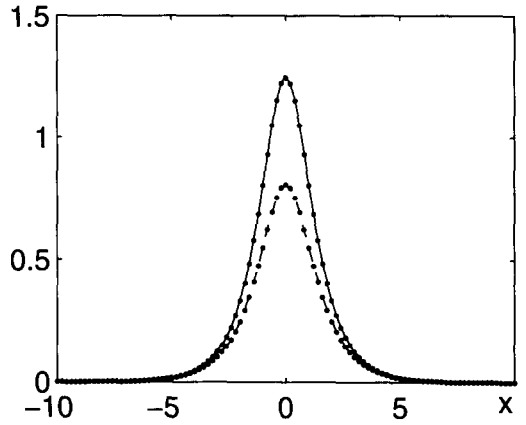

Fig. 1. A solitary wave in family D_1. The parameter values are $\beta = \frac{2}{3}$ and $\omega = 0.9$. Solid curve: r_1; dashed curve: r_2; dotted curves: variational approximation (3.11) and (3.12).

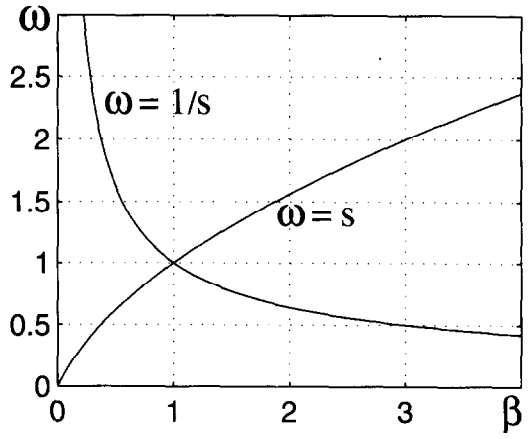

Fig. 2. Family D_1's parameter region.

$r_2(0)/r_1(0)$ increases continuously from zero to infinity. Family D_1 includes the exact solitary waves (2.7) and (2.8) as well as the wave and daughter wave solutions of the type (2.13) and (2.17). This family has been studied before [5,6,8–10,13]. Its associated family is itself.

Next we set out to analytically investigate the solitary waves in family D_1. If the point (β, ω) is close to one of the two boundary curves (3.1) and (3.2) in Fig. 2, then the corresponding solitary wave is a wave and daughter wave solution. Its exact analytical expression, including the amplitude of the daughter wave, can be obtained perturbatively. Suppose (β, ω) is close to the curve (3.1), then the asymptotic expansion of the solution is

$$r_1 = \sqrt{2}\,\operatorname{sech} x + \epsilon^2\phi_1(x) + \epsilon^4\phi_2(x) + \ldots, \tag{3.3a}$$

$$r_2 = \epsilon\,\operatorname{sech}^s x + \epsilon^3\psi_1(x) + \epsilon^5\psi_2(x) + \cdots, \tag{3.3b}$$

$$\omega = s + \epsilon^2\omega^{(1)} + \epsilon^4\omega^{(2)} + \cdots, \tag{3.3c}$$

where s is given by (2.16) and $\epsilon \ll 1$. When (3.3) is substituted into Eqs. (2.3) and terms of the same order in ϵ are collected, the equations for ϕ_n and ψ_n ($n \geq 1$) can be obtained. The equation for ϕ_1 is

$$\phi_{1xx} - \phi_1 + 6\,\mathrm{sech}^2 x\phi_1 = -\sqrt{2}\,\beta\,\mathrm{sech}^{2s+1} x, \tag{3.4}$$

whose solution is

$$\phi_1 = \frac{\sqrt{2}}{4} s \left\{ (1-2s)\mathrm{sech}\, x \tanh x \int_0^x \mathrm{sech}^{2s} \xi \, \mathrm{d}\xi - \mathrm{sech}^{2s+1} x \right\}. \tag{3.5}$$

The equation for ψ_1 is

$$\psi_{1xx} - s^2\psi_1 + 2\beta\,\mathrm{sech}^2 x\,\psi_1 = 2s\,\omega^{(1)}\mathrm{sech}^s x - \mathrm{sech}^{3s} x - 2\sqrt{2}\beta\,\mathrm{sech}^{s+1} x\,\phi_1. \tag{3.6}$$

In order for the solution ψ_1 to vanish as $x \to \pm\infty$, the solvability condition

$$\int_{-\infty}^{\infty} (2s\,\omega^{(1)}\mathrm{sech}^s x - \mathrm{sech}^{3s} x - 2\sqrt{2}\beta\,\mathrm{sech}^{s+1} x\phi_1)\mathrm{sech}^s x \, \mathrm{d}x = 0 \tag{3.7}$$

has to be satisfied. This condition determines $\omega^{(1)}$ to be

$$\omega^{(1)} = \frac{(1-s^3)\int_{-\infty}^{\infty} \mathrm{sech}^{4s} x \, \mathrm{d}x}{2s\int_{-\infty}^{\infty} \mathrm{sech}^{2s} x \, \mathrm{d}x}. \tag{3.8}$$

Eq. (3.8) shows that $\omega^{(1)}$ is positive when $0 < \beta < 1$ and negative when $\beta > 1$. This means that the wave and daughter wave solution (3.3) is to be found for $\omega > s$ when $0 < \beta < 1$ and for $\omega < s$ when $\beta > 1$. This agrees with our numerical findings. For fixed β, when such ω is given and close to s, the amplitude ϵ of the daughter wave r_2 can be estimated by Eqs. (3.3c) and (3.8). Higher-order corrections in expansion (3.3) can be obtained with a little more effort. If the point (β, ω) is close to the other boundary curve (3.2), the analytical expressions for the corresponding wave and daughter wave solutions can be deduced from the above results by the reciprocal relation (2.6) stated in the previous section.

If the point (β, ω) is not close to either of the two boundary curves (3.1) and (3.2) in Fig. 2, then the above results based on the perturbation method will be poor. In this case a different analytical method – the variational principle method – can be used. The Lagrangian form of Eqs. (2.3) is

$$\delta \int_{-\infty}^{\infty} \mathcal{L}(r_1, r_2)\, \mathrm{d}x = 0, \tag{3.9}$$

where the Lagrangian $\mathcal{L}$ is

$$\mathcal{L} = \tfrac{1}{2}r_1^4 - r_1^2 - r_{1x}^2 + \tfrac{1}{2}r_2^4 - \omega^2 r_2^2 - r_{2x}^2 + \beta r_1^2 r_2^2. \tag{3.10}$$

When an ansatz is assumed for the solutions r_1 and r_2 and is substituted into Eq. (3.9), a system of algebraic equations will be obtained for the ansatz parameters. Apparently this method is based on approximations. Its success depends on whether the chosen ansatz for the true solution is appropriate or not. In the present situation the solitary waves in family D_1 are symmetric and single-humped (see Fig. 1). Based on the information we have obtained so far we propose the following ansatz:

$$r_1 = c_1\,\mathrm{sech}\, x, \qquad r_2 = c_2\,\mathrm{sech}^{\omega} x \tag{3.11}$$

for the solutions when $\beta \leq 1$ and $\omega \leq 1$ or $\beta \geq 1$ and $\omega \geq 1$. When (3.11) is substituted into Eq. (3.9) and the variations with respect to c_1 and c_2 taken, two algebraic equations for c_1 and c_2 will be obtained. Solving these equations we get

$$c_1^2 = \frac{2\int_{-\infty}^{\infty} \operatorname{sech}^{4\omega} x\,dx - 3\beta\omega^3(\omega+1)\left[\int_{-\infty}^{\infty} \operatorname{sech}^{2\omega} x\,dx\right]^2/(2\omega+1)^2}{\int_{-\infty}^{\infty} \operatorname{sech}^{4\omega} x\,dx - 3\beta^2\omega^2\left[\int_{-\infty}^{\infty} \operatorname{sech}^{2\omega} x\,dx\right]^2/(2\omega+1)^2}, \tag{3.12a}$$

$$c_2^2 = \frac{2\omega(\omega^2+\omega-2\beta)\int_{-\infty}^{\infty} \operatorname{sech}^{2\omega} x\,dx/(2\omega+1)}{\int_{-\infty}^{\infty} \operatorname{sech}^{4\omega} x\,dx - 3\beta^2\omega^2\left[\int_{-\infty}^{\infty} \operatorname{sech}^{2\omega} x\,dx\right]^2/(2\omega+1)^2}, \tag{3.12b}$$

Some conclusions can be readily drawn from the above results. First, the boundary curve of the ansatz solution (3.11) in the parameter plane is

$$\omega^2 + \omega - 2\beta = 0, \tag{3.13}$$

where c_2 is equal to zero. This is the same as the exact boundary curve (3.1). Second, when $0 < \beta < 1$, the denominator in Eq. (3.12b) is always positive. In order for solution c_2 to exist, it is necessary that

$$\omega^2 + \omega - 2\beta > 0, \tag{3.14}$$

i.e. $\omega > s$. When $\beta > 1$, the denominator in Eq. (3.12b) along the boundary curve (3.1) becomes negative. Therefore, c_2 solution exists only if

$$\omega^2 + \omega - 2\beta < 0, \tag{3.15}$$

i.e. $\omega < s$. These results agree with the perturbation results and the numerical findings. Thirdly, when (β, ω) is close to the boundary curve (3.1), Eq. (3.12b) can be simplified as

$$\omega = s + kc_2^2 + O(c_2^4), \tag{3.16}$$

where

$$k = \frac{\int_{-\infty}^{\infty} \operatorname{sech}^{4s} x\,dx - 3\beta^2 s^2\left[\int_{-\infty}^{\infty} \operatorname{sech}^{2s} x\,dx\right]^2/(2s+1)^2}{2s\int_{-\infty}^{\infty} \operatorname{sech}^{2s} x\,dx}. \tag{3.17}$$

When comparing (3.16) and (3.17) with the perturbation results (3.3c) and (3.8), we see a slight difference between the first-order correction coefficients k and $\omega^{(1)}$. This discrepancy is caused by the approximation of the true r_1 and r_2 solutions with the ansatz (3.11). Actually for (β, ω) close to the boundary (3.1), the true solutions are given perturbatively by (3.3) and (3.5), which are slightly different from the ansatz (3.11). So a difference of order c_2^2 should be expected between (3.16) and (3.3c). But this difference is rather small. For instance, when $\beta = \frac{2}{3}$, Eqs. (3.8) and (3.17) give

$$\omega^{(1)} \approx 0.2439, \quad k \approx 0.2426, \tag{3.18}$$

which are very close. Lastly when $\beta = 1$ and $\omega = 1$, the denominators and numerators in Eqs. (3.12) are all zero, so expression (3.12) is no longer valid. Actually in this case the variational principle method gives only one equation for c_1 and c_2, which is

$$c_1^2 + c_2^2 = 2. \tag{3.19}$$

So the variational solutions are also (2.8) in agreement with the exact solutions.

The merit of the variational solution (3.11) and (3.12) is that it provides an approximate analytical expression for the r_1 and r_2 solution even if (β, ω) is not close to the boundary curve (3.1), i.e. the solution is not a wave and daughter wave solution. To check the accuracy of this solution we plotted it in Fig. 1 along with the numerically obtained true solution for $\beta = \frac{2}{3}$ and $\omega = 0.9$. The two solutions are almost identical. Such excellent agreement is actually shared for β and ω anywhere in the parameter region $0 < \beta \leq 1$, $s < \omega \leq 1$ and $\beta \geq 1$, $1 \leq \omega < s$. In the rest of the parameter region (see Fig. 2), the ansatz (3.11) is no longer appropriate. In this case the variational solution can be obtained from (3.11) and (3.12) by the reciprocal relation (2.6) mentioned in Section 2.

3.2. *Family D_2*

We call family D_2 as the family of solitary waves which is generated by the second wave and daughter wave solution of the approximate form (2.13) and (2.18). When $\beta = 2$ and $\omega = 0.7$, this wave and daughter wave solution is numerically determined and plotted in Fig. 3. In family D_2, the r_1 solution is symmetric and r_2 solution, anti-symmetric. In the parameter plane, family D_2's parameter region spreads out from the wave and daughter wave boundary

$$\omega = s - 1 = \tfrac{1}{2}(\sqrt{1 + 8\beta} - 3). \tag{3.20}$$

We have determined this region numerically and plotted its boundaries in Fig. 4. The boundaries consist of the following five curves:

(1) $\beta = 0$, $\omega \geq 1$;
(2) $\omega = 1/s = 2/(\sqrt{1 + 8\beta} - 1)$, $0 < \beta \leq 1$;
(3) curve L_1, $0 \leq \beta \leq 1$ (determined numerically);
(4) $\omega = 1$, $\beta \geq 1$;
(5) $\omega = s - 1 = \frac{1}{2}(\sqrt{1 + 8\beta} - 3)$, $\beta \geq 1$.

Near the boundary $\omega = s - 1$ ($\beta > 1$), the solutions are wave and daughter wave solutions as expected (see Fig. 3). As ω moves from the boundary $\omega = s - 1$ to $\omega = 1$, the r_2 amplitude gets larger, and the single r_1 pulse splits up into two (see Fig. 5(a)). Near the boundary $\omega = 1$ the solutions are two-peak pulses which appear to be two solitary waves (2.7) patched together (see Fig. 5(b)). As $\omega \to 1$, the distance between these two pulses goes to infinity. When β decreases from the boundary $\omega = s - 1$ ($1 < \beta < 3$) to curve L_1, the amplitudes of r_2's two

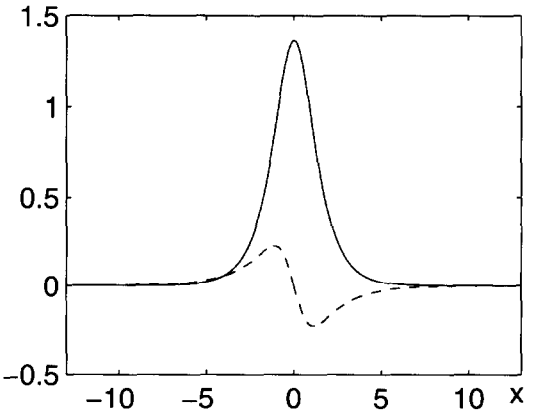

Fig. 3. A wave and daughter wave solution in family D_2. The parameter values are $\beta = 2$ and $\omega = 0.6$. Solid curve: r_1; dashed curve: r_2.

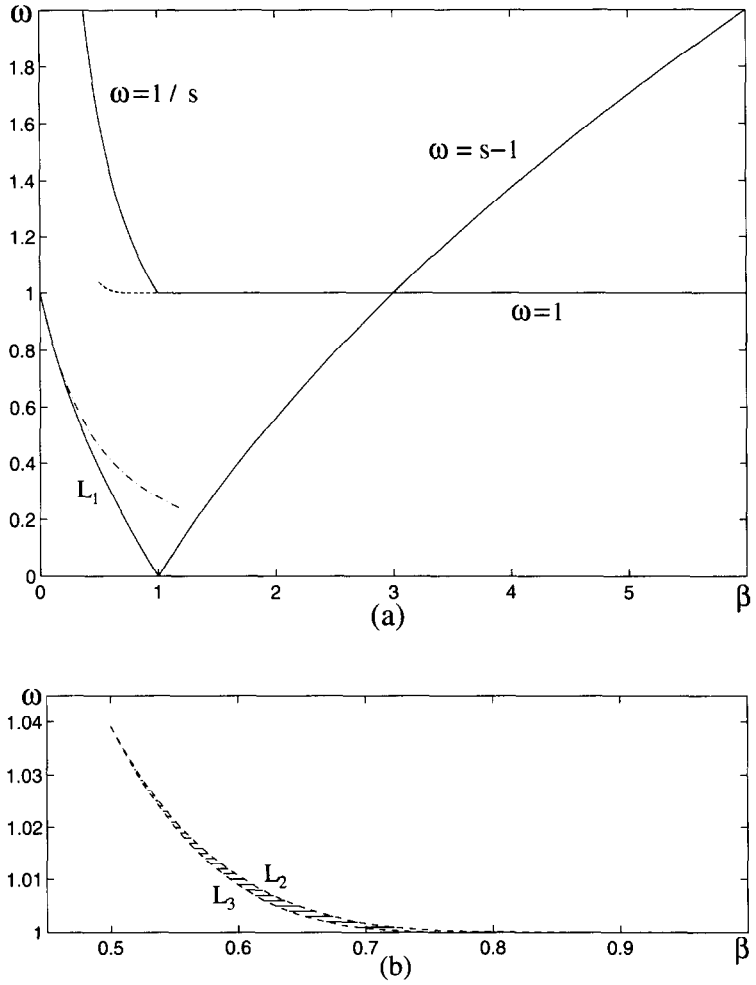

Fig. 4. (a) Family D_2's parameter region. The dash-dotted curve is the perturbative approximation (3.34) to the boundary curve L_1. (b) Enlargement of the thin crescent in (a) (shaded). In this region, three family D_2's solitary waves exist at each point.

pulses steadily increase, so does the distance between them. The single r_1 pulse, on the other hand, first splits up into two, then the two pulses merge again and become a single pulse. Near the boundary L_1, the r_1 solution has a single pulse in the middle, and the r_2 solution has two anti-symmetric pulses on the outside (see Fig. 5(c)). It appears that the solution is patched together by a solitary wave (2.4) and two other waves (2.5). As ω approaches L_1, the two r_2 pulses move to infinity. Near the boundary $\beta = 0$ ($\omega > 1$), the solution characteristics is essentially the same as that near L_1. When ω increases from boundary L_1 to $\omega = 1/s$, the single r_1 pulse splits up into two, which then are bound together with the two r_2 pulses. Later on, the amplitudes of the two r_1 pulses steadily decrease, while those of the r_2 pulses steadily increase. Near the boundary $\omega = 1/s$, the solutions appear to be patched together by two wave and daughter wave solutions of family D_1 (see Fig. 5(d)). This is not surprising since $\omega = 1/s$ is the boundary of family D_1's wave and daughter wave solutions with $r_1 \ll r_2$. As ω approaches the boundary $\omega = 1/s$ the amplitudes of the two r_1 pulses reduce to zero, and the distance between the two r_2 pulses tends to infinity. Family D_2 includes the exact solitary waves (2.9) (with $\Delta x = 0$) and (2.10) beside the wave and daughter wave solutions of the type (2.13) and (2.18). Its associated family is different from itself.

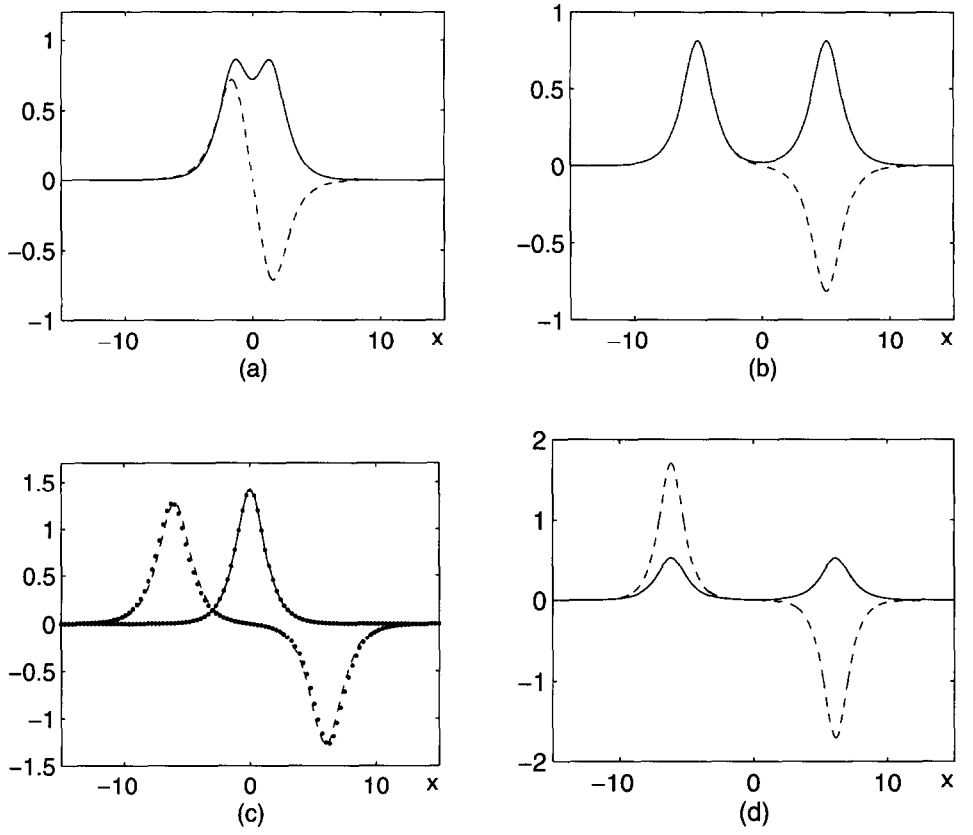

Fig. 5. Family D_2's solitary waves. Solid curves: r_1; dashed curves: r_2. The parameters values (β, ω) are (a) (2, 0.9); (b) (2, 0.9999); (c) (0.1, 0.9); (d) $(\frac{2}{3}, 1.25)$. In (c), the dotted curves are the leading order perturbative approximation (3.25) to the solution.

There is a further complication in family D_2's solitary waves. It turns out that in its parameter region, there is a very thin crescent (shown in Figs. 4(a) and (b)) where three family D_2's solutions exist at each point, while in the rest of the region only one solution exists. This crescent is bounded by two curves L_2 and L_3. Its two end points are $(\beta, \omega) \approx (0.50, 1.039)$ and $(1, 1)$. For fixed β between 0.50 and 1, as ω increases from 1 to curve L_2, the solution continuously varies. As L_2, a saddle-node bifurcation occurs. Above L_2, the solution disappears. Below it, a new solution appears. As ω turns back at L_2, the solution smoothly changes from one branch to the other. As ω decreases from L_2 to L_3, the solution changes continuously. At L_3, another saddle-node bifurcation occurs. Below it, the solution disappears. Above it, a new branch of solutions appears. As ω turns around at L_3, the solution moves from one branch to the other. Finally, as ω increases from L_3 to the boundary $\omega = 1/s$, the solution continuously changes and no more bifurcations occur. Because of the two saddle-node bifurcations, at each point in the crescent enclosed by L_2 and L_3, there are three family D_2's solutions.

To quantitatively illustrate the solution features in family D_2, we select $\beta = \frac{2}{3}$ and analyze in more detail. For each solitary wave in family D_2, when $|x| \to \infty$,

$$r_1 \longrightarrow a_1 e^{-|x|}, \qquad r_2 \longrightarrow -a_2 \operatorname{sgn}(x) e^{-\omega|x|}, \tag{3.21}$$

where a_1 and a_2 are two positive constants. A solitary wave in family D_2 is uniquely determined by the a_1 and a_2 values. For family D_2's solitary waves with $\beta = \frac{2}{3}$, these values against ω are plotted in Fig. 6(a). When $\beta = \frac{2}{3}$, the ω value on the boundary curve L_1 is approximately equal to 0.2417, and that on the boundary $\omega = 1/s$ is

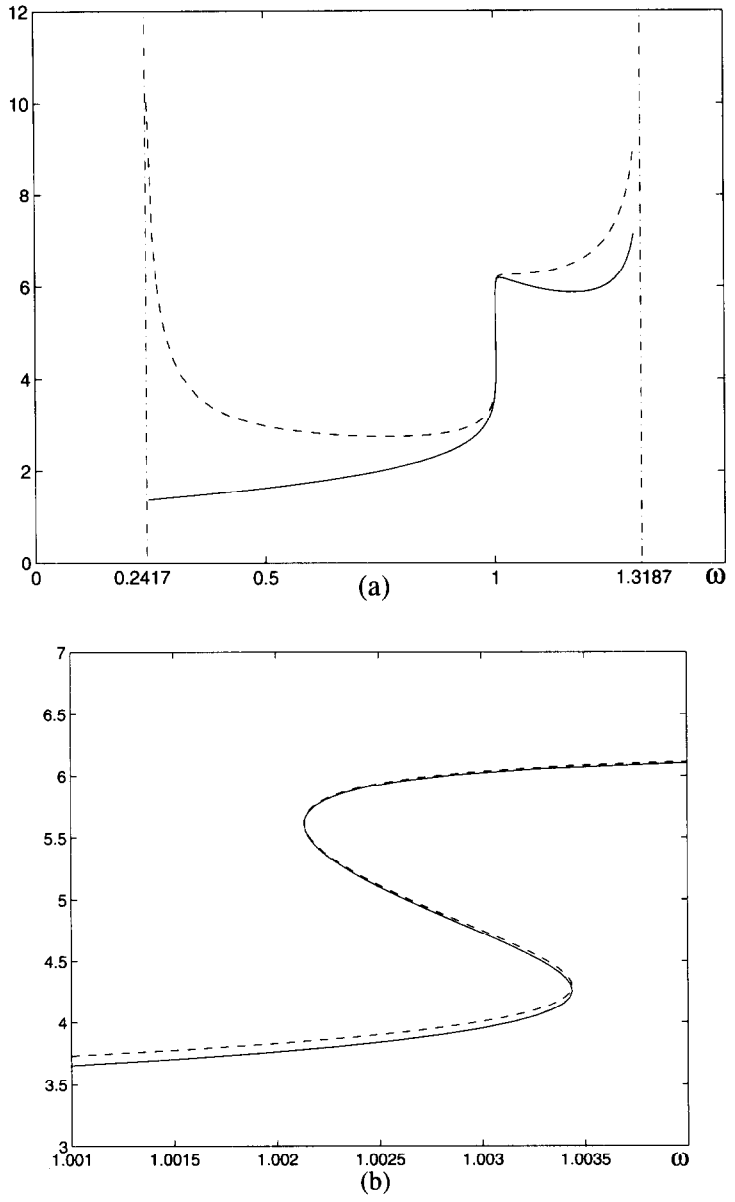

Fig. 6. (a) The a_1 and a_2 values of family D_2's solitary waves for $\beta = \frac{2}{3}$. Solid curves: $\ln(a_1)$; dashed curves: $\ln(a_2)/\omega$. (b) Enlargement of (a) at the vertical jump.

$2/(\sqrt{19/3} - 1) \approx 1.3187$. As $\omega \to 0.2417$, $a_1 \to$ constant, $a_2 \to \infty$, and the corresponding solitary waves appear to be patched by a r_1 pulse (2.4) and two r_2 pulses (2.5) (see Fig. 5(c)). As $\omega \to 1.3187$, both a_1 and a_2 approach infinity. Meanwhile $a_1 \ll a_2$. The corresponding solitary waves appear to be patched by two wave and daughter wave solutions of family D_1 (see Fig. 5(d)). More interestingly, there is a large vertical jump near $\omega = 1$ in Fig. 6(a). When this jump is enlarged in Fig. 6(b), we see an "s" shaped configuration. The two saddle-node bifurcations occur at $\omega \approx 1.00345$ and 1.0021. At each ω value between 1.0021 and 1.00345, we find three solitary waves belonging to family D_2. This type of solution behavior is precisely that which happens in the thin crescent in Fig. 4(b). The

two bifurcation points $(\beta, \omega) = (\frac{2}{3}, 1.00345)$ and $(\frac{2}{3}, 1.0021)$ are on curves L_2 and L_3, respectively. The vertical jump in Fig. 6(a) is quite a surprise. Over a very short ω interval [1.0021, 1.00345], the values of a_1 and a_2 exhibit a dramatic change. This indicates that the parameter dependence of family D_2's solitary waves is quite sensitive. As β approaches either of the two end points 0.50 and 1, we found that the length of the ω interval of the jump shrinks to zero (see Fig. 4(b)). But there is a major difference here. As β decreases to 0.50, this vertical jump gradually disappears. On the contrary, as β increases to 1, the jump amount approaches infinity. This indicates that when β is closer to 1, the vertical jump as seen in Fig. 6(a) will be sharper, and the parameter dependence of the solitary waves will be more sensitive.

Next we analytically study the solitary waves in family D_2. If (β, ω) is close to the boundary $\omega = s - 1$ in the parameter plane, we have known that the solutions are wave and daughter wave solutions whose approximated expressions are (2.13) and (2.18). Their exact expressions, including the amplitude of the daughter wave r_2, can be obtained perturbatively. This procedure is similar to the one we employed for the wave and daughter waves in family D_1, so only the results are reported here. The asymptotic expansion of the solution is

$$r_1 = \sqrt{2}\,\operatorname{sech} x + \epsilon^2\phi_1(x) + \epsilon^4\phi_2(x) + \cdots, \tag{3.22a}$$

$$r_2 = \epsilon\,\operatorname{sech}^s x \sinh x + \epsilon^3\psi_1(x) + \epsilon^5\psi_2(x) + \cdots, \tag{3.22b}$$

$$\omega = s - 1 + \epsilon^2\omega^{(1)} + \epsilon^4\omega^{(2)} + \cdots, \tag{3.22c}$$

where $\epsilon \ll 1$. The function $\phi_1(x)$ and coefficient $\omega^{(1)}$ are found to be

$$\phi_1 = \frac{\sqrt{2}}{4}\left\{(3-s)\operatorname{sech} x \tanh x \int_0^x \operatorname{sech}^{2(s-1)}\theta \, d\theta - \operatorname{sech}^{2s-1} x\right\}, \tag{3.23}$$

and

$$\omega^{(1)} = \frac{(2-s)(7s^2 - 7s + 3)}{8(s-1)(2s-1)} \frac{\int_{-\infty}^{\infty} \operatorname{sech}^{4s} x \, dx}{\int_{-\infty}^{\infty} \operatorname{sech}^{2s} x \, dx}. \tag{3.24}$$

Eq. (3.24) shows that when $1 < \beta < 3$, i.e. $1 < s < 2$, $\omega^{(1)}$ is positive; when $\beta > 3$, i.e. $s > 2$, $\omega^{(1)}$ is negative. In the parameter plane, this means that the wave and daughter wave solutions (2.13) and (2.18) exist for $\omega > s - 1$ when $1 < \beta < 3$ and $\omega < s - 1$ when $\beta > 3$. This result is consistent with our numerical findings. Higher-order corrections in (3.22) can be obtained systematically with more effort, but it will not be pursued here.

Another type of solitary waves for which the perturbation method can be applied is the one which appears to be patched by a single r_1 pulse (2.4) and two r_2 pulses (2.5) (see Fig. 5(c)). In the parameter region such solutions are located near the boundaries $\beta = 0$ and L_1. The asymptotic expansion of these solutions is

$$r_1 = \sqrt{2}\,\operatorname{sech} x + \beta e^{-x_0} f_1(x) + o(\beta e^{-x_0}), \tag{3.25a}$$

$$r_2 = \sqrt{2}\,\omega(s_+ - s_-) + \epsilon e^{-\omega x_0} g_1(x) + o(\epsilon e^{-\omega x_0}), \tag{3.25b}$$

where

$$s_+ \equiv \operatorname{sech} \omega(x + x_0), \qquad s_- \equiv \operatorname{sech} \omega(x - x_0), \tag{3.26}$$

$$\epsilon = \begin{cases} \beta, & \omega < 2, \\ e^{-\omega x_0}, & \omega \geq 2, \end{cases} \tag{3.27}$$

$$\max\{f_1(x)\} = O(1), \qquad \max\{g_1(x)\} = O(1), \tag{3.28}$$

and $x_0 > 0$ is the central position of r_2's right hand pulse. We require that $x_0 \gg 1$ and $\beta \ll 1$ so that the above asymptotic series is uniformly valid. We also require that $\omega \geq \frac{1}{2}$ for technical reasons. When expansion (3.25) is substituted into Eqs. (2.3) and higher-order terms neglected, the equations for f_1 and g_1 are found to be

$$f_{1xx} + (6\,\mathrm{sech}^2 x - 1) f_1 = -2\sqrt{2}\,\omega^2\,\mathrm{sech}\, x(\mathrm{s}_+ - \mathrm{s}_-)^2 \mathrm{e}^{x_0}, \tag{3.29a}$$

$$g_{1xx} + \{6\omega^2(\mathrm{s}_+ - \mathrm{s}_-)^2 - \omega^2\} g_1 = 2\sqrt{2}\,\omega(\beta\,\mathrm{sech}^2 x - 3\omega^2 \mathrm{s}_+\mathrm{s}_-)(\mathrm{s}_+ - \mathrm{s}_-)\mathrm{e}^{\omega x_0}/\epsilon. \tag{3.29b}$$

At first sight, it appears that the right-hand side of Eq. (3.29b) may not be an order 1 function. Actually it is due to the later results. In order for the solutions f_1 and g_1 to vanish as $x \to \pm\infty$, certain solvability conditions need to be satisfied. The condition for Eq. (3.29a) is

$$\int_{-\infty}^{\infty} \mathrm{sech}\, x(\mathrm{s}_+ - \mathrm{s}_-)^2\,\mathrm{sech}\, x \tanh x\, \mathrm{d}x = 0, \tag{3.30}$$

which is satisfied automatically. The condition for Eq. (3.29b) is

$$\int_{-\infty}^{\infty} 2\sqrt{2}\,\omega(\beta\,\mathrm{sech}^2 x - 3\omega^2 \mathrm{s}_+\mathrm{s}_-)(\mathrm{s}_+ - \mathrm{s}_-)\mathrm{s}_+\mathrm{t}_+\mathrm{e}^{\omega x_0}\,\mathrm{d}x = 6\omega^2\epsilon \int_{-\infty}^{\infty} \mathrm{s}_+\mathrm{t}_+\mathrm{s}_-(\mathrm{s}_- - 2\mathrm{s}_+) g_1\,\mathrm{d}x, \tag{3.31}$$

where $\mathrm{t}_+ \equiv \tanh \omega(x + x_0)$. It is easy to show that when $x_0 \gg 1$ and $\beta \ll 1$, the right-hand side of Eq. (3.31) is exponentially smaller than either of the two terms in the left-hand side. So asymptotically the solvability condition (Eq. (3.31)) reduces to

$$\beta = \frac{\int_{-\infty}^{\infty} 3\omega^2 \mathrm{s}_+^2 \mathrm{t}_+ \mathrm{s}_-(\mathrm{s}_+ - \mathrm{s}_-)\,\mathrm{d}x}{\int_{-\infty}^{\infty} \mathrm{sech}^2 x\, \mathrm{s}_+\mathrm{t}_+(\mathrm{s}_+ - \mathrm{s}_-)\,\mathrm{d}x}. \tag{3.32}$$

This equation implicitly determines x_0 as a function of β and ω. It is asymptotically accurate if $x_0 \gg 1$ and $\beta \ll 1$. When $\beta = 0.1$ and $\omega = 0.9$, Eq. (3.32) gives $x_0 = 6.1836$. In this case, the asymptotic solution (3.25), to the leading order, is plotted in Fig. 5(c) together with the numerically obtained true solution. Good agreement can be observed. As $\omega x_0 \to \infty$, to the leading order Eq. (3.32) becomes

$$\beta \longrightarrow \begin{cases} \dfrac{\omega^2 \mathrm{e}^{-2(\omega-1)x_0}}{\int_{-\infty}^{\infty} \mathrm{sech}^2\,\omega x\, \mathrm{e}^{2x}\,\mathrm{d}x}, & \omega > 1, \\ \dfrac{1}{4x_0}, & \omega = 1, \\ \dfrac{\omega}{\int_{-\infty}^{\infty} \mathrm{sech}^2 x\,(\mathrm{e}^{2\omega x} - 1)\,\mathrm{d}x}, & \omega < 1. \end{cases} \tag{3.33}$$

Therefore in the parameter plane the boundary for the solutions (3.25) is

$$\beta = \begin{cases} 0, & \omega \geq 1, \\ \dfrac{\omega}{\int_{-\infty}^{\infty} \mathrm{sech}^2 x(\mathrm{e}^{2\omega x} - 1)\,\mathrm{d}x}, & \omega < 1. \end{cases} \tag{3.34}$$

The graph of Eq. (3.34) for $\omega < 1$ is plotted in Fig. 4(a) (dash-dotted curve). When β is small, this curve is in good agreement with the true boundary curve L_1. When β gets large, the asymptotic expansion (3.25) and relation (3.32) both fail, therefore, it is not surprising that the graph of (3.34) and the curve L_1 separate.

The solitary waves examined above can also be studied by the variational principle method. For this purpose we choose the ansatz as

$$r_1 = \sqrt{2}\,\mathrm{sech}\,x, \tag{3.35a}$$

$$r_2 = \sqrt{2}\,\omega(s_+ - s_-), \tag{3.35b}$$

where s_+ and s_- are defined in Eq. (3.26). When this ansatz is substituted into the Lagrangian equation (3.9) and the variations with respect to x_0 taken, the equation for x_0 will be obtained. It turns out that this equation is exactly the same as Eq. (3.32) obtained before by the perturbation method, but the algebra is much simpler here. The drawback of this variational result is that it gives no indication as to when it is accurate and when it is not. In comparison, the answer to that question is clear in the perturbation result.

Some other types of solitary waves, such as the one shown in Fig. 5(d) when (β, ω) is close to the boundary $\omega = 1/s$ and the one shown in Fig. 5(b) when ω is close to 1 ($\beta > 1$), can also be studied by the perturbation method or the variational principle method in a similar way. But the details are omitted here.

3.3. Family D_3

We call family D_3 the family of solitary waves generated by the third wave and daughter wave solution of the approximate form (2.13) and (2.19). When $\beta = 4.5$ and $\omega = 0.7$, this wave and daughter wave solution is numerically determined and plotted in Fig. 7. In family D_3, both the r_1 and r_2 solutions are symmetric in x. Its parameter region spreads out from the wave and daughter wave boundary

$$\omega = s - 2 = \tfrac{1}{2}(\sqrt{1 + 8\beta} - 5). \tag{3.36}$$

We have numerically determined this region and plotted its boundaries in Fig. 8. The boundaries consist of the following six curves:

(1) $\omega = 1$, $1 \le \beta \le 3$;
(2) L_4, $3 \le \beta \lesssim 7.4$, (determined numerically);
(3) $\omega = s - 2 = \frac{1}{2}(\sqrt{1 + 8\beta} - 5)$, $\beta \gtrsim 7.4$;
(4) $\omega = 1$, $\beta \ge 6$;
(5) $\omega = s - 2$, $3 \le \beta \le 6$;
(6) L_5, $1 \le \beta \le 3$ (determined numerically).

Near the curve $\omega = s - 2$, the solutions are wave and daughter wave solutions whose approximate expressions are (2.13) and (2.19) (see Fig. 7). For any fixed ω, as β decreases from the boundary $\omega = s - 2$ ($3 \le \beta \le 6$) to L_5, the amplitude of the r_2 solution steadily increases, and the single r_1 pulse develops a shoulder (see Fig. 9(a)). Then this

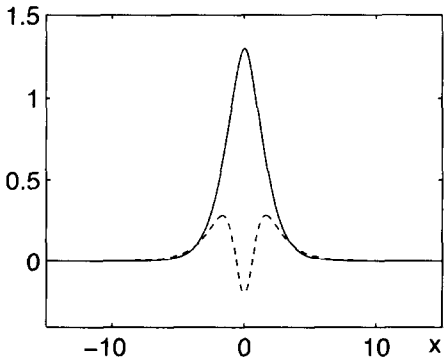

Fig. 7. A wave and daughter wave solution in family D_3. The parameter values are $\beta = 4.5$ and $\omega = 0.7$. Solid curve: r_1; dashed curve: r_2.

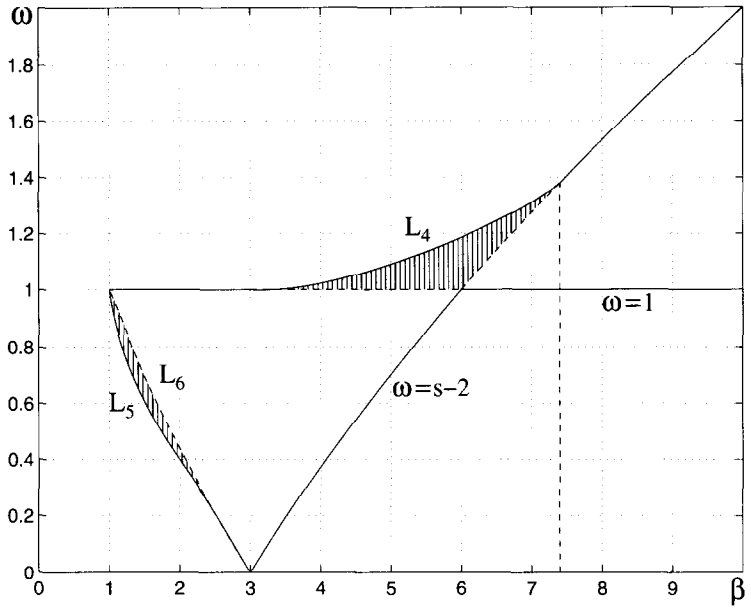

Fig. 8. Family D_3's parameter region. In the shaded region, two solitary waves belonging to family D_3 exist at each point.

shoulder gradually lowers while the two outer pulses in r_2 separate (see Fig. 9(c)). At L_5, a saddle-node bifurcation occurs. If β crosses L_5, the solution disappears. When β turns back and increases, the solution smoothly moves onto a new branch. When β moves from L_5 to the curve L_6, the shoulder in the r_1 pulse gradually vanishes, and r_2 becomes two isolated pulses separating apart (see Fig. 9(d)). Near L_6, the solution appears to be patched by a r_1 pulse (2.4) and two symmetric r_2 pulses (2.5). As β approaches L_6, the two r_2 pulses escape to infinity. As a result, for each point (β, ω) in the narrow strip enclosed by L_5 and L_6, two family D_3's solutions exist (see Figs. 9(c) and (d)). If the point (β, ω) approaches the boundary $\omega = 1$ $(1 < \beta < 3)$, the solution appears to be patched by three solitary waves of equal amplitudes (2.7) which separate further and further apart (see Fig. 9(b)). Now we fix β $(\beta \geq 3)$ and allow ω to vary. When $3 \leq \beta \lesssim 7.4$, close and above the curve $\omega = s - 2$, the solutions are wave and daughter wave solutions (see Fig. 7). As ω increases from the boundary $\omega = s - 2$ to L_4, the amplitudes of r_2's three pulses steadily increase, and the single r_1 pulse develops a shoulder. At L_4, a saddle-node bifurcation occurs. Above L_4, the solution disappears. Below it, another branch of solutions appears. As ω turns back at L_4 and decreases, the solution changes continuously from one branch to the other. Finally when ω moves down from L_4 to the line $\omega = 1$, both r_1 and r_2 develop into three waves of equal amplitudes (2.7), and the solution becomes similar to Fig. 9(b). As ω approaches 1, these pulses separate infinitely apart. In the above process we discover another interesting parameter region enclosed by the three curves L_4, $\omega = 1$ $(3 \leq \beta \leq 6)$ and $\omega = s - 2$ $(6 \leq \beta \lesssim 7.4)$ (see the upper shaded region in Fig. 8). In this "triangle" region, due to the saddle-node bifurcation at L_4, two solutions belonging to family D_3 exist at each point. This behavior is similar to that in the narrow strip enclosed by L_5 and L_6. When $\beta \gtrsim 7.4$, both the parameter region and the parameter dependence of the solitary waves become simple again. The wave and daughter wave solutions are now located near and below the boundary $\omega = s - 2$. As ω decreases from this boundary to the line $\omega = 1$, the solutions change smoothly from the wave and daughter wave solutions (see Fig. 7) to solutions patched by three waves of equal amplitudes (2.7) separating apart (see Fig. 9(b)).

For demonstration purpose, we now consider the two special cases $\beta = 2$ and $\beta = 5$ in more detail. As $|x| \to \infty$, the solitary waves in family D_3 have the following asymptotic behaviors:

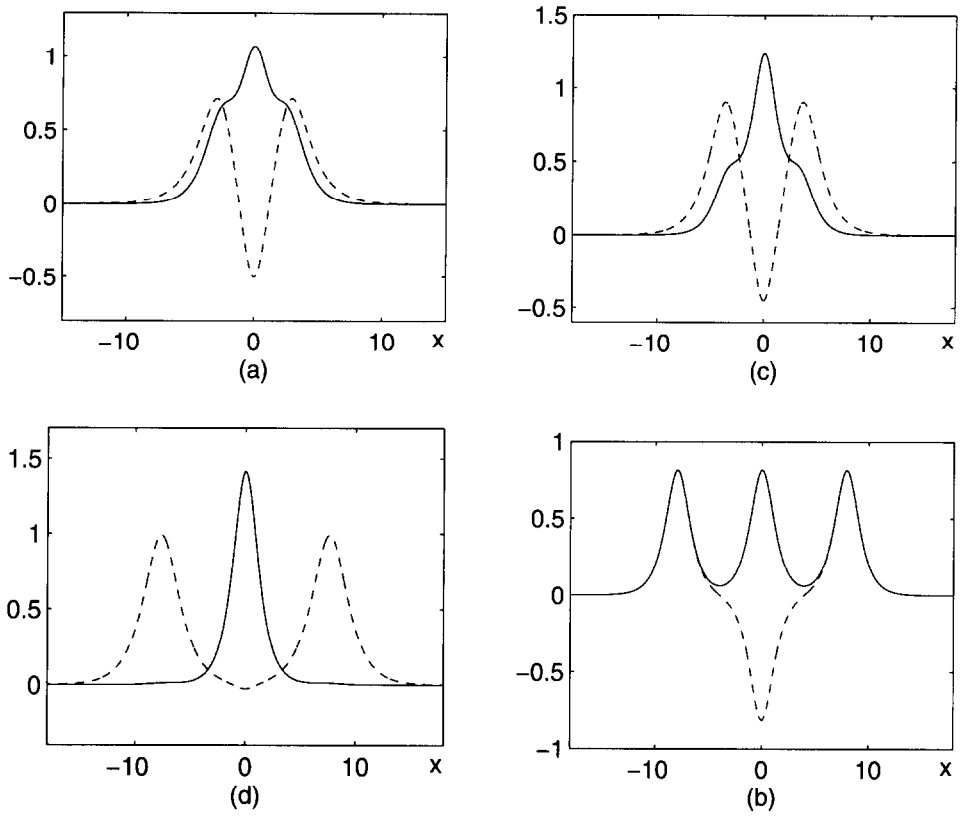

Fig. 9. Family D_3's solitary waves. The parameter values (β, ω) are (a) (2, 0.7); (b) (2, 0.999); (c) (1.42, 0.7); (d) (1.42, 0.7).

$$r_1 \to a_1 e^{-|x|}, \qquad r_2 \to a_2\, e^{-\omega|x|}, \tag{3.37}$$

where a_1 and a_2 are two positive constants. When $\beta = 2$, the a_1 and a_2 values of these solitary waves are plotted in Fig. 10. Observe that as $\omega \to 1$, $a_1 \to \infty$, $a_2 \to \infty$, and $a_1/a_2 \to 1$. In this case, the solution appears to be patched by three solitary waves of equal amplitudes (2.7) (see Fig. 9(b)). At $\omega \approx 0.40$ (which is on boundary L_5), a saddle-node bifurcation occurs. As $\omega \to 0.44$ (which is on curve L_6), $a_1 \to$ constant, $a_2 \to \infty$, and the corresponding solution appears to be patched by a r_1 pulse (2.4) and two r_2 pulses (2.5) (see Fig. 9(d)). Note from Fig. 10 that in the ω interval [0.40, 0.44], two family D_3's solutions exist. When $\beta = 5$, the a_1 and a_2 values are plotted in Fig. 11. When ω is near 0.7016 (which is on the boundary $\omega = s - 2$), $a_1 \approx 2\sqrt{2}$, $a_2 \ll 1$, and the solitary wave is a wave and daughter wave solution approximated by (2.13) and (2.19). At $\omega \approx 1.09$ (which is on boundary L_4), a saddle-node bifurcation occurs. As $\omega \to 1$, $a_1 \to \infty$, $a_2 \to \infty$, $a_1/a_2 \to 1$, and the corresponding solution is similar to Fig. 9(b). Again note from Fig. 11 that two family D_3's solutions exist in the ω interval [1, 1.09].

Next we analytically study family D_3's solitary waves. When the point (β, ω) lies close to the boundary $\omega = s - 2$, we have known that the solutions are wave and daughter wave solutions. Once again, the exact expressions for these solutions can be obtained by perturbation methods. The asymptotic expansion of such solutions is

$$r_1 = \sqrt{2}\,\mathrm{sech}\, x + \epsilon^2 \phi_1(x) + \epsilon^4 \phi_2(x) + \cdots, \tag{3.38a}$$

$$r_2 = \epsilon\,\{1 + 2(1-s)\sinh^2 x\}\mathrm{sech}^s x + \epsilon^3 \psi_1(x) + \epsilon^5 \psi_2(x) + \cdots, \tag{3.38b}$$

$$\omega = s - 2 + \epsilon^2 \omega^{(1)} + \epsilon^4 \omega^{(2)} + \cdots, \tag{3.38c}$$

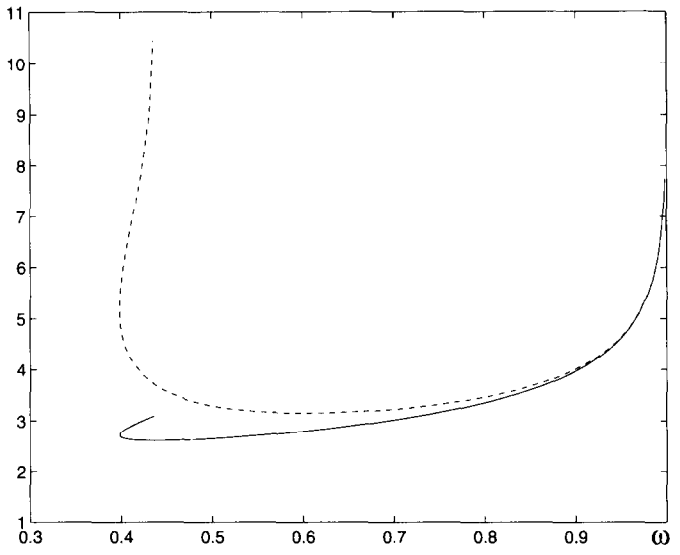

Fig. 10. The a_1 and a_2 values of family D_3's solitary waves for $\beta = 2$. Solid curve: $\ln(a_1)$; dashed curve: $\ln(a_2)/\omega$.

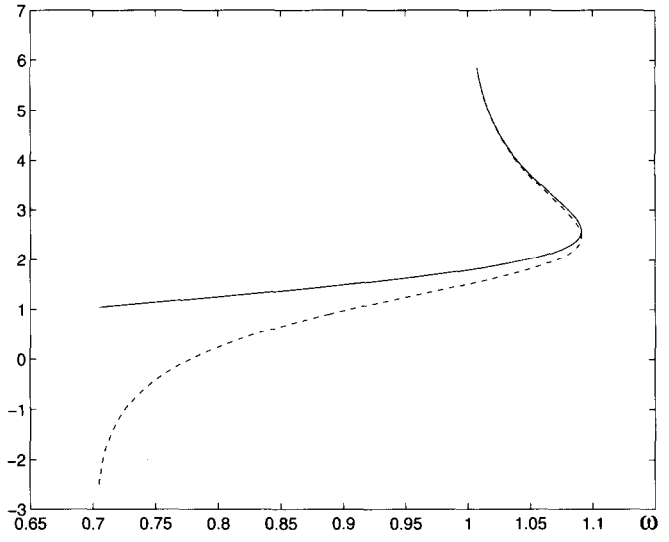

Fig. 11. The a_1 and a_2 values of family D_3's solitary waves for $\beta = 5$. Solid curve: $\ln(a_1)$; dashed curve: $\ln(a_2)/\omega$.

where $\epsilon \ll 1$. Following the procedure outlined before we find that

$$\phi_1 = \phi_1^{(a)}(x) + \phi_1^{(b)}(x)\operatorname{sech} x \tanh x, \tag{3.39}$$

where

$$\phi_1^{(a)} = \tfrac{1}{4}\sqrt{2}\{4(s-1)^2(s+1)\operatorname{sech}^{2s-3} x - s(2s-1)^2\operatorname{sech}^{2s-1} x\}, \tag{3.40}$$

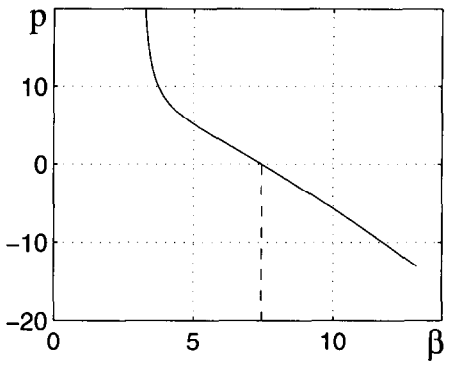

Fig. 12. The graph of the function $p(s)$ against β.

and

$$\phi_1^{(b)} = \tfrac{1}{2}\sqrt{2}\int_0^x \{2(s^2-1)(2s^2-5s+4)\operatorname{sech}^{2s-4}\theta - s(s-1)(2s-1)^2\operatorname{sech}^{2s-2}\theta\}\,d\theta. \tag{3.41}$$

The coefficient $\omega^{(1)}$ is given by

$$\omega^{(1)} = p(s)\frac{\int_{-\infty}^{\infty}\operatorname{sech}^{4s}x\,dx}{\int_{-\infty}^{\infty}\operatorname{sech}^{2s}x\,dx}, \tag{3.42}$$

where $p(s)$ is a rational function of s whose expression is quite complicated. In Fig. 12 we plotted the graph of p against β. The function p has one root $\beta \approx 7.4384$. It is positive when $3 \le \beta < 7.4384$ and negative when $\beta > 7.4384$. This indicates that the wave and daughter wave solutions (3.38) exist for $\omega > s-2$ when $3 \le \beta < 7.4384$ and for $\omega < s-2$ when $\beta > 7.4384$. This result is in excellent agreement with the parameter region (Fig. 8) numerically obtained. When (β, ω) is close to the curve L_6 or $\omega = 1$, the solitary waves can also be determined by the perturbation methods or the variational principle method. The details will not be given here.

Families of solitary waves which are generated by Eq. (2.13) and higher-mode daughter wave solutions (2.14) can be classified in a similar manner. It is expected that their parameter regions and parameter dependence will be even more interesting and complicated. In this paper we will not pursue further in this direction.

A notable feature of family D_3's parameter region is that it does not cross over the vertical line $\beta = 1$ into the strip $0 < \beta < 1$. The reason is that on the line $\beta = 1$, all the symmetric solitary waves are located at the single point $(\beta, \omega) = (1, 1)$ (see Eqs. (2.8) and (2.9)), and those solutions belong to family D_1. By similar reasons we conclude that the parameter regions of solution families generated by higher-mode wave and daughter wave solutions are all confined to the right-hand side of the vertical line $\beta = 1$. On the other hand, for families of solitary waves (other than D_1, D_2 and D_2's associated family) which exist for $0 < \beta < 1$, their parameter regions will not cross over the line $\beta = 1$ into the region $\beta > 1$ either. Such families of solutions are also abundant and will be reported elsewhere.

4. Stability of the solitary waves

One application of the above classification of the solitary waves in Eqs. (1.1) is to determine the stability of those waves. In one family, any two solitary waves can continuously deform from one to the other as the parameters vary. Therefore they generally have the same stability behaviors (if no stability bifurcations occur). As a result, if

the stability of one solitary wave in a family is known, then the stability of that whole family can be heuristically deduced. First we discuss family D_1's stability. Family D_1 includes the solitary waves (2.7) and (2.8) (with $\beta = 1$ and $\omega = 1$). When $\beta = 1$, Eqs. (1.1) are the Manakov equations and are exactly integrable [21]. It has been shown that the solitary waves (2.8) are actually solitons, and thus are stable. We then expect that all family D_1's solitary waves are stable. This is confirmed in our previous work [5,6]. In [5] we established the stability of the solitary waves (2.7) by perturbation methods. In [6] we proved the stability of all single-hump solitary waves by examining the complete eigenmodes of the linearized equations of (1.1) around those single-hump waves. Next we discuss family D_2's stability. This family includes the solitary waves (2.9) (with $\beta = 1$ and $\Delta x = 0$) and (2.10), and has been shown numerically to be unstable in [13]. In the special case when $\beta = 1$, it is well known that (2.9) is a two-soliton state and is thus unstable, consistent with the above result. The instability of this family is further confirmed by our own numerical studies on the evolution of many solitary waves in this family (also see [5]). But it should be noted that the instability characteristics of family D_2's solitary waves are not all the same. In fact, for the two-soliton state (2.9) ($\beta = 1$), the small disturbances governed by the linearized equations of (1.1) around (2.9) grow linearly with time. For other solitary waves in family D_2, we found numerically that the small disturbances grow exponentially with time. For instance, for the solitary wave (2.10) ($\beta = 3$) with $\Delta x = 1$, we found that the small disturbances exponentially grow with the maximum growth rate approximately equal to 0.54. These different instability behaviors indicate that, under small perturbations, the two-soliton state (2.9) takes much longer time to disintegrate than the other solitary waves in family D_2. Lastly, we discuss family D_3. To determine its stability, we selected one of its solitary waves with $\beta = 2$ and $\omega = 0.7$ (shown in Fig. 9(a)) and used it as the initial condition in Eqs. (1.1). The time evolution of this wave was numerically computed and plotted in Fig. 13. We can see that it is unstable to small numerical round off error disturbances. We also studied the time evolution of many other solitary waves in various parts of the parameter region of this family and found that they are never stable. Thus we deduce that family D_3 is unstable. Furthermore, we found that all the solitary waves in family D_3 whose time evolution we numerically investigated are exponentially unstable, i.e. small disturbances of these waves grow exponentially. For instance, for the solitary wave shown in Fig. 9(a), its small disturbances exponentially grow with the maximum growth rate approximately equal to 0.35. To determine the stability of the solution families generated by higher-mode wave and daughter wave solutions, the same method can be used, and we expect that those families are all unstable. These results support our previous conjecture [5] that only the family D_1 of symmetric and single-humped solitary waves is stable.

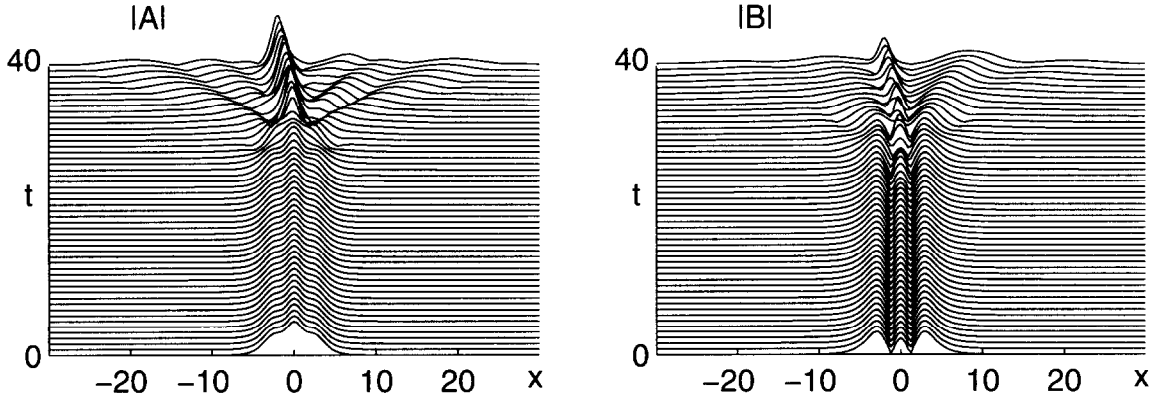

Fig. 13. Instability of a solitary wave in family D_3. This wave, with $\beta = 2$, $\omega = 0.7$ (see Fig. 9(a)), is used as the initial condition for Eqs. (1.1). The subsequent time evolutions for $|A|$ and $|B|$ are shown in the upper and lower graphs, respectively.

5. Discussion

The families of solitary waves studied in this paper signify the complexity of the solution structures in the nonlinear eigenvalue system (2.3). The parameter regions of these families (see Figs. 2, 4 and 8) are novel, intricate and unexpected. The big jump in the solution coefficients over a very short parameter interval (see Fig. 6(a)) reveals the surprisingly sensitive dependence of the solitary waves on the parameters. Moreover, the small parameter regions where two or more solitary waves belonging to the same family exist at each point seem to be unpredictable. This indicates that the solution structures of the nonlinear eigenvalue system (2.3) is much more complicated than that of any linear eigenvalue system.

In this paper, we only classified the families of symmetric and anti-symmetric solitary waves which are generated by the wave and daughter wave solutions. Actually, there are also countably infinite families of symmetric or anti-symmetric solitary waves which do not fall into that category. In addition, there are abundant asymmetric solitary waves exemplified by the solutions (2.9). Studies on such solitary waves can be found in [7].

Acknowledgements

This work was supported in part by the National Science Foundation under the grant DMS-9622802.

References

[1] D.J. Benney and A.C. Newell, The propagation of nonlinear wave envelopes, J. Math. and Phys. 46 (1967) 133.
[2] G.J. Roskes, Some nonlinear multiphase interactions, Stud. Appl. Math. 55 (1976) 231.
[3] C.R. Menyuk, Nonlinear pulse propagation in birefringent optical fibers, IEEE J. Quantum Electron, QE-23 (1987) 174.
[4] G.P. Agrawal, Nonlinear Fiber Optics (Academic Press, New York, 1995).
[5] J. Yang and D.J. Benney, Some properties of nonlinear wave systems, Stud. Appl. Math. 96 (1996) 111.
[6] J. Yang, Vector solitons and their internal oscillations in birefringent nonlinear optical fibers, Stud. Appl. Math. 98 (1997) 61.
[7] J. Yang, Multiple permanent-wave trains in nonlinear systems, Stud. Appl. Math. (1997), to appear.
[8] V.K. Mesentsev and S.K. Turitsyn, Stability of vector solitons in optical fibers, Opt. Lett. 17 (1992) 1497.
[9] D.J. Kaup, B.A. Malomed and R.S. Tasgal, Internal dynamics of a vector soliton in a nonlinear optical fiber, Phys. Rev. E 48 (1993) 3049.
[10] M. Haelterman and A.P. Sheppard, The elliptically polarized fundamental vector soliton of isotropic Kerr media, Phys. Lett. A 194 (1994) 191.
[11] M. Haelterman and A.P. Sheppard, Bifurcation phenomena and multiple soliton-bound states in isotropic Kerr media, Phys. Rev. E 49 (1994) 3376.
[12] M. Haelterman, A.P. Sheppard and A.W. Snyder, Bound-vector solitary waves in isotropic nonlinear dispersive media, Opt. Lett. 18 (1993) 1406.
[13] Y. Silberberg and Y. Barad, Rotating vector solitary waves in isotropic fibers, Opt. Lett. 20 (1995) 246.
[14] N.J. Balmforth, Solitary waves and homoclinic orbits, Ann. Rev. Fluid Mech. 27 (1995) 335.
[15] N.N. Akhmediev, A.V. Buryak, J.M. Soto-Crespo and D.R. Andersen, Phase-locked stationary soliton states in birefringent nonlinear optical fibers, J. Opt. Soc. Am. B 12 (1995) 434.
[16] B. Buffoni and E. Sere, A global condition for quasi-random behavior in a class of conservative systems, Comm. Pure Appl. Math. 49 (1996) 285.
[17] W.D. Kalies and R.C.A.M. VanderVorst, Multitransition homoclinic and heteroclinic solutions of the extended Fisher–Kolmogorov equation, CDSNS Report # 231, Georgia Institute of Technology (1995).
[18] P.H. Rabinowitz, Homoclinic and heteroclinic orbits for a class of Hamiltonian systems, Calc. Var. 1: 1–36.
[19] L.D. Landau and E.M. Lifshitz, Quantum Mechanics: non-relativistic theory, (Pergamon Press, Oxford, 1977).
[20] D.J. Kaup, T.I. Lakoba and B.A. Malomed, Asymmetric solitons in mismatched dual-core optical fibers, INS Report # 271 ,Clarkson University (1996).
[21] S.V. Manakov, On the theory of two-dimensional stationary self-focusing of electromagnetic waves, Sov. Phys. JETP 38 (1974) 248–253.